Immunity
Article

Control of Intestinal Homeostasis, Colitis, and Colitis-Associated Colorectal Cancer by the Inflammatory Caspases

Jeremy Dupaul-Chicoine,[1,6] Garabet Yeretssian,[2,6] Karine Doiron,[2] Kirk S.B. Bergstrom,[3] Christian R. McIntire,[1] Philippe M. LeBlanc,[4] Charles Meunier,[1] Claire Turbide,[5] Philippe Gros,[1,5] Nicole Beauchemin,[1,5] Bruce A. Vallance,[3] and Maya Saleh[1,2,*]

[1]Department of Biochemistry, McGill University, Montreal, Quebec H3G 1Y6, Canada
[2]Department of Medicine, McGill University, Montreal, Quebec H3G 0B1, Canada
[3]Division of Gastroenterology, University of British Columbia and BC Children's Hospital, Vancouver, BC V6T 1Z4, Canada
[4]Department of Microbiology and Immunology, McGill University, Montreal, Quebec H3A 2B4, Canada
[5]Goodman Cancer Centre, McGill University, Montreal, Quebec H3A 1A3, Canada
[6]These authors contributed equally to this work
*Correspondence: maya.saleh@mcgill.ca
DOI 10.1016/j.immuni.2010.02.012

SUMMARY

Inflammatory caspases are essential effectors of inflammation and cell death. Here, we investigated their roles in colitis and colorectal cancer and report a bimodal regulation of intestinal homeostasis, inflammation and tumorigenesis by caspases-1 and −12. *Casp1*$^{-/-}$ mice exhibited defects in mucosal tissue repair and succumbed rapidly after dextran sulfate sodium administration. This phenotype was rescued by administration of exogenous interleukin-18 and was partially reproduced in mice deficient in the inflammasome adaptor ASC. *Casp12*$^{-/-}$ mice, in which the inflammasome is derepressed, were resistant to acute colitis and showed signs of enhanced repair. Together with their increased inflammatory response, the enhanced repair response of *Casp12*$^{-/-}$ mice rendered them more susceptible to colorectal cancer induced by azoxymethane (AOM)+DSS. Taken together, our results indicate that the inflammatory caspases are critical in the induction of inflammation in the gut after injury, which is necessary for tissue repair and maintenance of immune tolerance.

INTRODUCTION

The innate immune system provides first-line defenses against invading microbial organisms and endogenous danger signals by activating pathways that mediate tissue repair, inflammation, and microbial clearance. This is especially important in the intestinal mucosa in which pattern recognition receptors (PRRs) function to protect against microbial intrusion while maintaining epithelial barriers in the presence of commensal microorganisms. The need to maintain tolerance to commensal bacteria, which present a permanent threat of invasion after mechanical or immunological breach, requires a robust innate immunity network at intestinal mucosal surfaces. Bacterial sensing by PRRs is increasingly recognized to be critical for intestinal homeostasis and tissue repair after damage (Brown et al., 2007; Rakoff-Nahoum et al., 2004). Experimental animal models have demonstrated that depletion of the commensal microflora or deletion of the Toll-like receptor (TLR)-interleukin-1 (IL-1) and IL-18 receptor adaptor, MyD88, render animals highly susceptible in response to wounding of the epithelium with either irradiation or dextran sulfate sodium (DSS), a sulfated polysaccharide known to be directly toxic to colonic epithelium (Kitajima et al., 1999; Rakoff-Nahoum et al., 2004). In addition to TLRs, nucleotide-binding oligomerization domain containing 2 (NOD2) has been recently shown to be involved in controlling DSS-induced pathology. Notably, administration of the NOD2 agonist muramyl didpeptide (MDP) to mice was shown to confer protection from acute DSS-induced injury (Watanabe et al., 2008). NOD2 stimulation leads to the activation of MAP kinase and NF-κB signaling pathways, and the latter has been extensively studied in the context of chemical injury and colitis (Nenci et al., 2007). Together, these studies suggest that innate immune signaling triggered by the commensal bacteria-TLR or NOD-NF-κB axis is necessary for tissue homeostasis and immune tolerance.

Although physiologic levels of inflammation are protective, excessive inflammation is deleterious and is at the basis of inflammatory bowel disease (IBD) and inflammation-promoted colorectal cancer (CRC). CRC is a frequent form of malignancy and a major cause of death in the Western hemisphere. It arises spontaneously or as a result of chronic inflammation. IBD including ulcerative colitis and Crohn's disease are associated with an elevated risk of CRC (Clevers, 2004). It is believed that a break in tolerance to the commensal bacteria is at the basis of IBD pathogenesis. When commensal bacteria breach the intestinal epithelial barrier, they trigger a state of chronic inflammation, which is believed to be directly responsible for the neoplastic transformation of the overlying intestinal epithelium (Balkwill and Mantovani, 2001; Clevers, 2004). Production of cytokines together with that of matrix-degrading enzymes, growth

factors, and reactive oxygen species promote tumorigenesis by creating a microenvironment favoring intestinal epithelial cell proliferation, cell survival, and invasiveness.

Although the role of the NF-κB signaling pathway in CRC has been explored, the contribution of the inflammasome and the inflammatory caspases to intestinal homeostasis, colitis, and CRC is not clear. The search for the molecular mechanisms required for the activation of the inflammatory caspases led to the identification of the NOD-like family of molecules (nucleotide-binding domain and leucine-rich repeat containing molecules [NLRs]). NLRs are large cytosolic PRRs that, upon sensing microbial or danger signals, assemble inflammasomes and activate inflammatory caspases (Mariathasan and Monack, 2007; McIntire et al., 2009). Caspases-1, -4, -5, and -12 in humans, and caspases-1, -11, and -12 in rodents, are termed "inflammatory" on the basis of their ability to regulate the production of the proinflammatory cytokines IL-1β and IL-18. Caspase-1, the main effector inflammatory caspase, directly processes its cytokine substrates from proforms into mature biologically active forms, whereas caspase-12 is a repressor of the inflammasome and a molecular "brake" on caspase-1 activity (Yeretssian et al., 2008).

Accumulating evidence points to a critical role of the inflammasome and the inflammatory caspases in intestinal homeostasis and colitis. A recent report has identified single-nucleotide polymorphisms (SNPs) in a regulatory region downstream of the human *NLRP3* gene, which were found to be associated with Crohn's disease susceptibility in individuals of European descent. SNPs in this region result in decreased NLRP3 expression and dampened IL-1 family cytokine production (Villani et al., 2009). Of these cytokines, IL-18 is the most relevant as it has been suggested to contribute to intestinal epithelial cell regeneration as well as to chronic inflammation in IBD. In response to DSS-induced injury, IL-18 deficiency has been shown to result in severe colitis (Pizarro et al., 1999; Sivakumar et al., 2002; Takagi et al., 2003). Paradoxically, excessive IL-1 and IL-18 production has also been linked to morbidity and mortality in response to DSS colitis. It has been demonstrated that the autophagy protein ATG16L1 (autophagy-related 16-like 1), which is implicated in Crohn's disease, negatively regulates the inflammasome and that mice that lack ATG16L1 in hematopoeitic cells hyperproduce IL-1β and IL-18 and are susceptible to DSS colitis (Saitoh et al., 2008). Thus, it appears that IL-18 exerts a dual role in intestinal homeostasis and colitis. Early in the mucosal immune response, its expression by IECs and lamina propria mononuclear cells is suggested to mediate a cytoprotective role, but under chronic inflammation its excessive production results in deleterious effects (Reuter and Pizarro, 2004).

In this report, we describe a role for the caspase-1 inflammasome in epithelial cell regeneration and tissue repair after injury. We show that caspase-1-deficient mice were extremely susceptible to DSS-induced injury succumbing very early on compared to wild-type animals. This phenotype was primarily ascribed to lack of IL-18 production by *Casp1*$^{-/-}$ mice, given that it was completely reversed by exogenous administration of this cytokine. Moreover, we show that regulation of caspase-1 function by caspase-12 was necessary for immune tolerance in the gut. *Casp12*$^{-/-}$ mice, in which the inflammasome is derepressed, were resistant to acute and chronic colitis and showed signs of exaggerated epithelial cell compensatory proliferation. Together with their increased inflammatory response, the enhanced repair response of *Casp12*$^{-/-}$ mice rendered them more susceptible to colorectal cancer induced by azoxymethane (AOM)+DSS. Altogether, our results indicate that the inflammatory caspases are critical regulators of intestinal homeostasis and that deregulation of the caspase-1-caspase-12 axis of inflammation leads to severe colitis and colitis-associated CRC.

RESULTS

Caspase-1 Is Required for Tissue Repair in DSS-Induced Injury

Bacterial recognition by TLRs and Nod proteins and subsequent signaling through the NF-κB pathway have been reported to be important in maintaining intestinal epithelial tissue integrity (Rakoff-Nahoum et al., 2004; Watanabe et al., 2008). To investigate the role of the inflammatory caspases and the inflammasome in intestinal homeostasis, we subjected wild-type (WT), *Casp1*$^{-/-}$, *Casp12*$^{-/-}$, and *Asc*$^{-/-}$ mice to an experimental model of tissue injury and colitis. We hypothesized that the inflammasome and caspase-1 activity contributed to inflammation during colitis and that *Casp1*$^{-/-}$ mice would be protected from colitis. To assess their response, we administered dextran sulfate sodium (DSS) to mice in their drinking water for 5 days and then allowed the animals to recover with clean drinking water for an additional 4 days. Contrary to our hypothesis, *Casp1*$^{-/-}$ mice were extremely susceptible to this treatment and began to die on day 5 after DSS. By day 9 all of the *Casp1*$^{-/-}$ mice had died (Figure 1A). In sharp contrast, all WT, *Asc*$^{-/-}$, and *Casp12*$^{-/-}$ mice survived over this time course (Figure 1A and data not shown). The body weight of *Casp1*$^{-/-}$ mice steadily decreased and by day 8, *Casp1*$^{-/-}$ mice had lost more than 20% of their initial body weight (Figure 1B). In contrast and similar to WT mice, the body weight of *Casp12*$^{-/-}$ mice remained constant throughout the experiment, whereas *Asc*$^{-/-}$ mice had an intermediate phenotype and lost 10% of their body weight by day 8 (Figure 1B). *Casp1*$^{-/-}$ mice developed severe diarrhea and rectal bleeding starting on day 5 (Figure 1C) and showed severe signs of colitis including drastic shortening of the colon length at necropsy (Figure 1D and Figure S1A available online).

Mice of all genotypes displayed epithelial erosion on day 5 (Figure S1B). However, *Casp1*$^{-/-}$ mice displayed more severe signs of injury (Figures 2A–2D and Figures S1B and S1C). By day 8, WT and *Casp12*$^{-/-}$ mice exhibited regeneration of the intestinal epithelium (Figures 2A–2C), whereas *Asc*$^{-/-}$ mice had some remaining erosions, but unlike *Casp1*$^{-/-}$ mice, showed signs of re-epithelialization (Figures 2A–2C and Figure S1C). In contrast, *Casp1*$^{-/-}$ mice showed no improvement from day 5 to day 8, and few if any crypts were found throughout their distal colons on day 8 (Figures 2A–2D). Labeling of epithelial cell tight junctions by claudin-3 staining revealed normal expression and localization. In contrast, a defect in intestinal epithelial restitution was evident in *Casp1*$^{-/-}$ mice (Figure 2C and Figure S1C). This was consistent with reduced intestinal epithelial cell proliferation as revealed by proliferating cell nuclear antigen (PCNA) staining (Figure 2B). Quantification of PCNA-positive cells per 50-well-oriented crypts evaluated/mouse

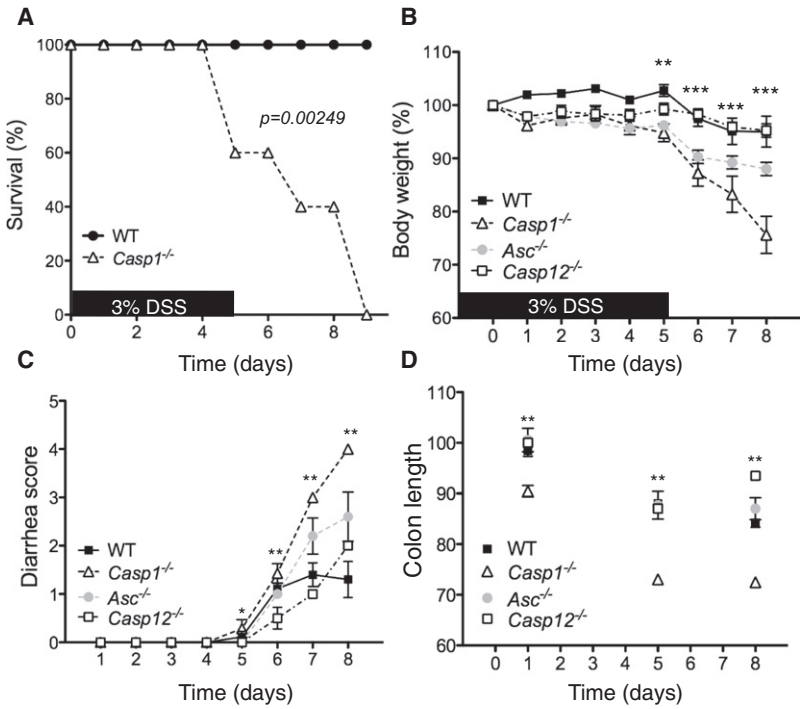

Figure 1. *Casp1*$^{-/-}$ Mice Are Highly Susceptible to Acute Dextran Sulfate Sodium Treatment

(A) WT and *Casp1*$^{-/-}$ mice were given 3% DSS in their drinking water for 5 days, then given regular drinking water for an additional 3 days (days 6–8). Difference in survival was determined with Kaplan-Meier analysis. This experiment was repeated twice with similar results. In each experiment, a group of five to seven mice was used per genotype.

(B) Body weight loss of WT, *Casp1*$^{-/-}$, *Asc*$^{-/-}$ and *Casp12*$^{-/-}$ mice treated with DSS as in (A) and weighed daily. Data represent the mean ± SEM of n = 8 mice/genotype. p values were calculated with ANOVA; **p < 0.01, ***p < 0.001.

(C) Stool consistency and intestinal bleeding were monitored on daily basis and diarrhea was scored for each mouse. Diarrhea was graded on a scale of 0–4 as described in the Experimental Procedures. Data represent the means ± SEM. p values were calculated with ANOVA; *p < 0.05, **p < 0.01.

(D) Colon length of DSS-treated mice was measured on days 1, 5, and 8 after the start of DSS treatment. Data represent the means ± SEM. p values were calculated with ANOVA; **p < 0.01.

("well-oriented" was defined as the crypt lumen being present from the top to the bottom of the crypt) indicated that whereas *Casp1*$^{-/-}$ mice had impaired IEC proliferation, *Casp12*$^{-/-}$ mice showed signs of exaggerated tissue repair (Figure 2E) with hyperplastic crypts (Figures 2A–2D) and improved restitution (Figure S1C). Interestingly, unlike *Casp1*$^{-/-}$ mice, *Asc*$^{-/-}$ mice did not have impairment in these processes (Figures 2A–2C and Figure S1B). To confirm the histopathological observations, we examined epithelial tissue disruption and permeability by a quantitative measurement, feeding mice on day 8 with FITC-dextran and quantifying fluorescence in the serum 4 hr after gavage. Figure 2F shows a significant increase of plasma FITC fluorescence in *Casp1*$^{-/-}$ mice compared to WT mice. *Asc*$^{-/-}$ mice had a trend toward increased fluorescence; however, their difference from WT mice was not significant (Figure 2F). These results indicated that the caspase-1 inflammasome is required to induce intestinal epithelial cell regeneration and tissue repair after injury and that the milder phenotype of *Asc*$^{-/-}$ mice could be ascribed to its dual function in activating the inflammasome while inhibiting the NF-κB pathway (Mariathasan et al., 2004; Stehlik et al., 2002).

Increased Inflammation and NF-κB Activation in the Colon of DSS-Treated *Casp1*$^{-/-}$ Mice

To assess the severity and involvement of inflammation in the colons of DSS-treated animals, we stained colon tissue sections for neutrophil (Gr-1), macrophage (F4/80), and T lymphocyte (CD4) infiltration. On day 5 after DSS treatment, there was no evident difference in leukocyte infiltration among the genotypes (Figures 3A–3C), despite the marked difference in morbidity and mortality (Figure 1). On day 8, colon sections from *Casp1*$^{-/-}$ mice displayed a drastic increase in Gr-1, F4/80, and CD4-positive cell numbers compared to those of all other genotypes under study (Figures 3A–3C). Significant inflammation was evident in 75%–100% of the colon of *Casp1*$^{-/-}$ mice, whereas its involvement was less than 25% of the colon of WT animals and between 26%–50% in *Asc*$^{-/-}$ mice (Figure 3D). Consistently, the acute phase protein serum amyloid A (SAA), a marker of colitis, was released at highest concentrations in the serum of *Casp1*$^{-/-}$ mice on day 5 of the treatment, compared to WT and *Asc*$^{-/-}$ mice (Figure 3E). On day 8, the titers of SAA in the serum were saturating, masking differences among genotypes.

We next examined activation of the NF-κB pathway in the colons of DSS-treated mice. Figure 3F depicts an immunoblot of total colonic lysates that shows a robust induction of the NF-κB-target gene IκBα in lysates of *Casp1*$^{-/-}$ mice compared to those of WT or *Casp12*$^{-/-}$ mice. *Asc*$^{-/-}$ mice had intermediate amounts of IκBα. The induction of IκBα correlated well with the severity of tissue damage and inflammation observed in the different mouse genotypes and suggested that the amplified inflammatory response in the colon of *Casp1*$^{-/-}$ mice was partially attributable to increased NF-κB activation. To determine whether the enhanced inflammatory response in lesioned tissue of *Casp1*$^{-/-}$ mice was due to impaired host defense in these mice, we used fluorescent in situ hybridization (FISH) staining to label colon sections for the presence of commensal bacteria. Our results indicated that caspase-1 deficiency not only abrogated the tissue repair response but also resulted in a defect in controlling commensal bacterial invasion: labeled bacteria were frequently observed in the lamina propria of colon sections derived from *Casp1*$^{-/-}$ mice but to a much lesser extent in those of WT, *Asc*$^{-/-}$, or *Casp12*$^{-/-}$ mice at lesioned sites (Figure 3G). Consistently, quantification of bacterial content in the colons, mesenteric lymph nodes, and spleens of DSS-treated mice by 16S rRNA qPCR revealed enhanced bacterial invasion in tissues derived from *Casp1*$^{-/-}$ mice compared to WT mice (Figure 3H).

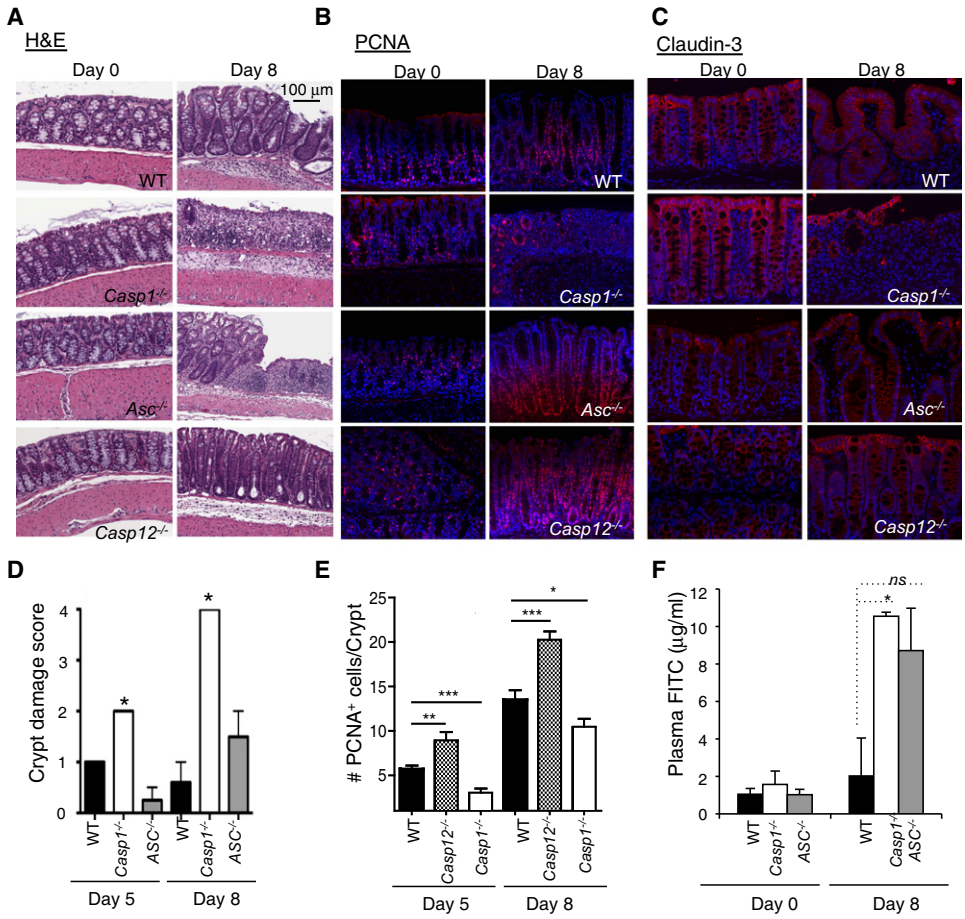

Figure 2. *Casp1*$^{-/-}$ Mice Have Impaired Epithelial Cell Regeneration and Tissue Repair after DSS Injury

(A) Hematoxylin and eosin (H&E) staining of colon sections derived from WT, *Casp1*$^{-/-}$, *Asc*$^{-/-}$, and *Casp12*$^{-/-}$ mice on days 0 and 8 after the start of DSS treatment (magnification 100×).

(B and C) Immunofluorescence was performed on colon sections derived from WT, *Casp1*$^{-/-}$, *Asc*$^{-/-}$, and *Casp12*$^{-/-}$ mice on days 0 and 8 for examination of proliferating cells (PCNA) (B) and tight junction (Claudin-3) (C); (magnification 100×).

(D) Histopathology scores evaluating the tissue involvement of crypt damage in WT, *Casp1*$^{-/-}$, and *Asc*$^{-/-}$ mice on days 5 and 8 after the start of DSS treatment. Results represent means ± SEM. Student's t test was performed for comparison of scores of *Casp1*$^{-/-}$ or *Asc*$^{-/-}$ mice to those of WT mice; *$p < 0.05$.

(E) Quantification of the numbers of PCNA^{+} cells shown in (B). On average, 50-well-oriented crypts were scored/mouse; "well-oriented" was defined as the crypt lumen being present from top to bottom of the crypt.

(F) Plasma FITC-dextran concentrations on day 8 in WT, *Casp1*$^{-/-}$, and *Asc*$^{-/-}$ mice, 4 hr after oral gavage of FITC-dextran (400 μg/g of body weight), are shown. Results represent means ± SEM. Student's t test was used for statistical analysis. *$p < 0.05$; *ns*, nonsignificant.

Altogether, our results suggest that during chemical-induced injury, caspase-1 plays a role in limiting mucosal damage by promoting regeneration of crypts and surface epithelia, thereby blocking excessive stimulation of lamina propria immune cells by luminal bacteria and inhibiting the production of chemotactic factors. Moreover, caspase-1 is required to control the numbers of commensal bacteria that leak into sites of colonic injury. These two caspase-1 dependent functions may be key in hindering the vicious cycle of inflammation caused by unregulated interactions between host tissues and the luminal microbiota.

IL-18 Production by Intestinal Epithelial Cells Is Critical for the Induction of Tissue Repair

To investigate the molecular basis of the impaired epithelial regeneration in caspase-1-deficient mice, we first quantified the concentrations of IL-1β and IL-18 in the serum of DSS-treated animals at different time points throughout the experiment. Interestingly, IL-1β concentrations in the serum increased minimally after DSS treatment (data not shown). In contrast, IL-18 production was highly induced in the sera of WT mice on days 5 and 8 after DSS treatment (Figure 4A). IL-18 is a key cytokine produced in a caspase-1-dependent manner; thus not surprisingly very little IL-18 was detected in the sera of *Casp1*$^{-/-}$ mice. In contrast, *Asc*$^{-/-}$ mice, which displayed an intermediate amount of DSS-induced colon tissue damage, had little production of IL-18 on day 5 but regained IL-18 production by day 8 (Figure 4A). It has been previously shown that IL-18 is essential for the early phase of wound healing, both in cutaneous wound models as well as in response to DSS (Kämpfer et al., 1999; Takagi et al., 2003). Moreover, both *Il18*$^{-/-}$ and

IL-18 receptor-deficient mice are susceptible to DSS colitis, developing a severe disease associated with high mortality and histopathological abnormalities similar to that in *Casp1*$^{-/-}$ mice (Takagi et al., 2003). The induction of IL-18 in WT mice, but not in *Casp1*$^{-/-}$ mice, on days 5 and 8 after DSS treatment suggested that IL-18 might mediate the caspase-1-dependent tissue repair response after injury. To test this hypothesis, we examined the effect of exogenous administration of recombinant IL-18 (rIL-18) on the phenotype of *Casp1*$^{-/-}$ mice in response to acute DSS treatment. We injected *Casp1*$^{-/-}$ mice with 0.05 μg rIL-18 or PBS daily on days 0, 1, and 2 post-DSS. Interestingly, this regimen completely reversed the *Casp1*$^{-/-}$ mice susceptibility phenotype given that 100% of the rIL-18-injected *Casp1*$^{-/-}$ animals survived the DSS treatment and maintained a stable body weight compared to PBS-treated *Casp1*$^{-/-}$ controls (Figure 4B). The cytoprotective effect of rIL-18 was evident when examining colon lengths at necropsy (Figure S2A), quantifying bacterial invasion in the colon with 16S rRNA qPCR (Figure 4C) as well as histologically (Figure 4D).

Previous studies investigating the role of MyD88 in tissue repair after DSS administration indicated an important contribution of myeloid cells to this response (Pull et al., 2005; Rakoff-Nahoum et al., 2004). To explore the role of myeloid cells in IL-18 production and stimulation of epithelial regeneration, we performed adoptive transfer of the myeloid compartment from WT mice into *Casp1*$^{-/-}$ mice during the course of DSS treatment. This treatment did not improve the *Casp1*$^{-/-}$ mice survival rate or body weight loss (data not shown). A slight amelioration was seen macroscopically, given that *Casp1*$^{-/-}$ mice that received the adoptive transfer had longer colons at necropsy compared to *Casp1*$^{-/-}$ control mice (Figure S2B). Histologically, although the colon tissue sections of *Casp1*$^{-/-}$ mice with adoptive transfer had residual crypts left as compared to *Casp1*$^{-/-}$ mice (Figure 4E), the colon was highly damaged as compared to colons from *Casp1*$^{-/-}$ mice treated with rIL-18 (Figure 4D). To further investigate the cell population involved in the production of IL-18, we isolated and purified IECs and different lamina propria cell populations (macrophages, dendritic cells [DCs], and lymphocytes) from untreated and colitic colons at different time points after injury and quantified IL-18 secretion by ELISA. IECs seem to be the primary source of IL-18 production after the DSS injury (Figure 4F). This is consistent with the lack of rescue by adoptive transfer of myeloid cells (Figure 4E) and with previous studies reporting IL-18 expression and localization predominantly to IECs of colons from Crohn's disease patients (Pizarro et al., 1999).

Caspase-12 Deficiency Enhances the Promotion of Colitis-Associated CRC

Caspase-12 is a dominant-negative regulator of the caspase-1 inflammasome and NOD-NF-κB pathways (Saleh et al., 2004; Saleh et al., 2006; LeBlanc et al., 2008). Although *Casp12*$^{-/-}$ mice reacted similarly to WT mice when allowed to recover from an acute DSS-induced injury (Figure 1) and exhibited signs of improved repair (Figure 2), they had an increased inflammatory response compared to WT animals (Figures 5A and 5B). Immunoblot analysis of colonic lysates on days 5 and 8 after DSS treatment revealed enhanced induction of multiple NF-κB target genes, including those that encode COX2, Bcl-xl, and cyclin D1 in the colons of *Casp12*$^{-/-}$ mice compared to those of WT animals (Figure 5A). Furthermore, colons of DSS-treated *Casp12*$^{-/-}$ mice hyperproduced proinflammatory cytokines and chemokines, such as IL-1β and KC (Figure 5B). It is now well recognized that physiological inflammation is beneficial in the intestine, whereas exaggerated production of inflammatory mediators contributes to colitis pathology. We therefore hypothesized that whereas the inflammatory response of *Casp12*$^{-/-}$ mice rendered them resistant to acute DSS treatment, hyperactivation of this response would lead to susceptibility in response to sustained treatment with DSS. Consistent with our hypothesis, *Casp12*$^{-/-}$ mice were highly susceptible to sustained DSS with less than 20% of the mice surviving by day 15 after DSS treatment as compared to 80% survival for WT mice (Figure S3). These data indicated that the hyperinflammatory state induced by the absence of the negative dominant role of caspase-12 on inflammation was deleterious, leading to severe colitis. We next subjected the *Casp12*$^{-/-}$ mice to an established model of chronic colitis induced by three cycles of low concentrations of DSS separated by a break week of clean drinking water (Figure 5C). In contrast to the sustained treatment, the chronic DSS regimen allows for epithelial regeneration and tissue repair during the break weeks and is a more representative model of chronic colitis. Consistent with their response to acute DSS treatment and their enhanced tissue repair phenotype, *Casp12*$^{-/-}$ mice were more resistant to chronic colitis compared to WT animals, gaining weight by the end of the experiment as compared to WT mice that lost 5% of their initial body weight (Figure 5C).

Because chronic inflammation is linked to tumorigenesis, we next sought to determine the contribution of the inflammatory caspases to colitis-associated CRC. We therefore subjected *Casp12*$^{-/-}$ mice to an AOM+DSS regimen. AOM or azoxymethane is a procarcinogen, which upon metabolic activation in the liver and the distal colon induces the formation of O^6-methyl-guanine (Pegg, 1984). Both WT and *Casp12*$^{-/-}$ mice survived the treatment and had similar body weights throughout the experiment, with the *Casp12*$^{-/-}$ mice gaining weight by the end of the experiment as compared to WT mice (Figure 5D), a result consistent with that obtained in the chronic DSS experiments (Figure 5C). Strikingly, *Casp12*$^{-/-}$ mice had a much higher tumor burden than WT mice (Figure 5E). As expected, AOM induced tumors at the distal end of the colon in WT mice (Figure 5E). *Casp12*$^{-/-}$ mice, in contrast, had tumors distributed from the distal end to the medial part of the colon, thereby demonstrating increased tumorigenesis (Figure 5E). *Casp12*$^{-/-}$ mice had 17 tumors on average, whereas WT mice had six (Figure 5G). The higher tumor burden was also highlighted by the weights of the colons, which were heavier in *Casp12*$^{-/-}$ mice compared to WT mice (Figure 5F). In addition to the increase in tumor number, *Casp12*$^{-/-}$ mice had larger tumors, with more than 50% of the tumors being larger than 2 mm in diameter compared to 30% for WT mice (Figure 5H). Taken together, these results suggested that the inflammatory microenvironment created by *Casp12* deficiency enhanced tumor promotion and progression.

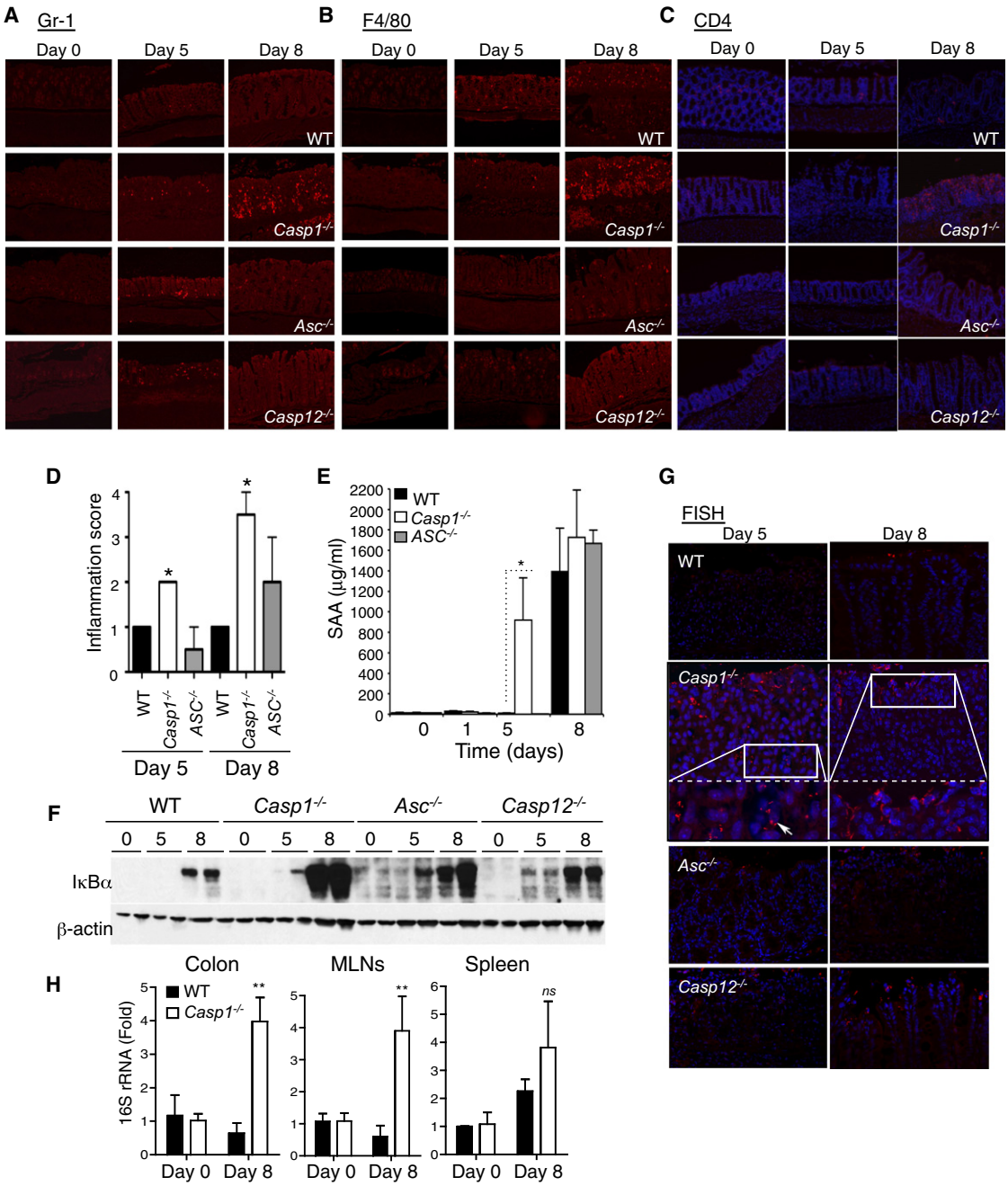

Figure 3. Enhanced Inflammation and NF-κB activation in DSS-Treated *Casp1*$^{-/-}$ Mice

(A–C) Immunofluorescence was performed on colon sections derived from WT, *Casp1*$^{-/-}$, *Asc*$^{-/-}$ and *Casp12*$^{-/-}$ mice on days 0, 5, and 8 for examination of neutrophil (Gr-1+ cells) (A), macrophage (F4/80+ cells) (B) and T lymphocyte (CD4+ cells) (C) infiltration; (magnification 100×).

(D) histopathology scores evaluating the tissue involvement of inflammation in WT, *Casp1*$^{-/-}$, and *Asc*$^{-/-}$ mice on days 5 and 8 after the start of DSS treatment. Results represent means ± SEM. Student's t test was performed for comparison of scores of *Casp1*$^{-/-}$ or *Asc*$^{-/-}$ mice to those of WT mice. *$p < 0.05$.

(E) Serum amyloid A (SAA) concentrations in the serum of mice on days 0, 1, 5, and 8 after DSS treatment were determined by ELISA. Data represent the mean ± SEM. *$p < 0.05$.

(F) Total protein lysates, prepared from colon tissues of WT, *Casp1*$^{-/-}$ *Asc*$^{-/-}$, and *Casp12*$^{-/-}$ mice on days 0 and 8 after DSS treatment, were analyzed for the induction of IκBα expression by western blotting. β-actin was used to control for equal loading.

(G) Invasion of commensal bacteria was assessed by labeling bacteria in colon sections of WT, *Casp1*$^{-/-}$, *Asc*$^{-/-}$, and *Casp12*$^{-/-}$ mice on days 5 and 8 after the start of DSS treatment with fluorescence in situ hybridization (FISH); 200× original magnification is shown. Tissues from *Casp1*$^{-/-}$ mice had the highest number of invading commensal bacteria in the lamina propria. Insets (corresponding to white boxes) are magnified 400× and show the presence of bacteria inside the cytosol of host cells (white arrow).

(H) RNA from colon, mesenteric lymph node (MLN), and spleen was isolated and bacterial content was measured by quantitative real-time PCR of 16S rRNA. Data represent means ± SEM of fold induction over untreated mice for each genotype (n = 4–7/genotype).

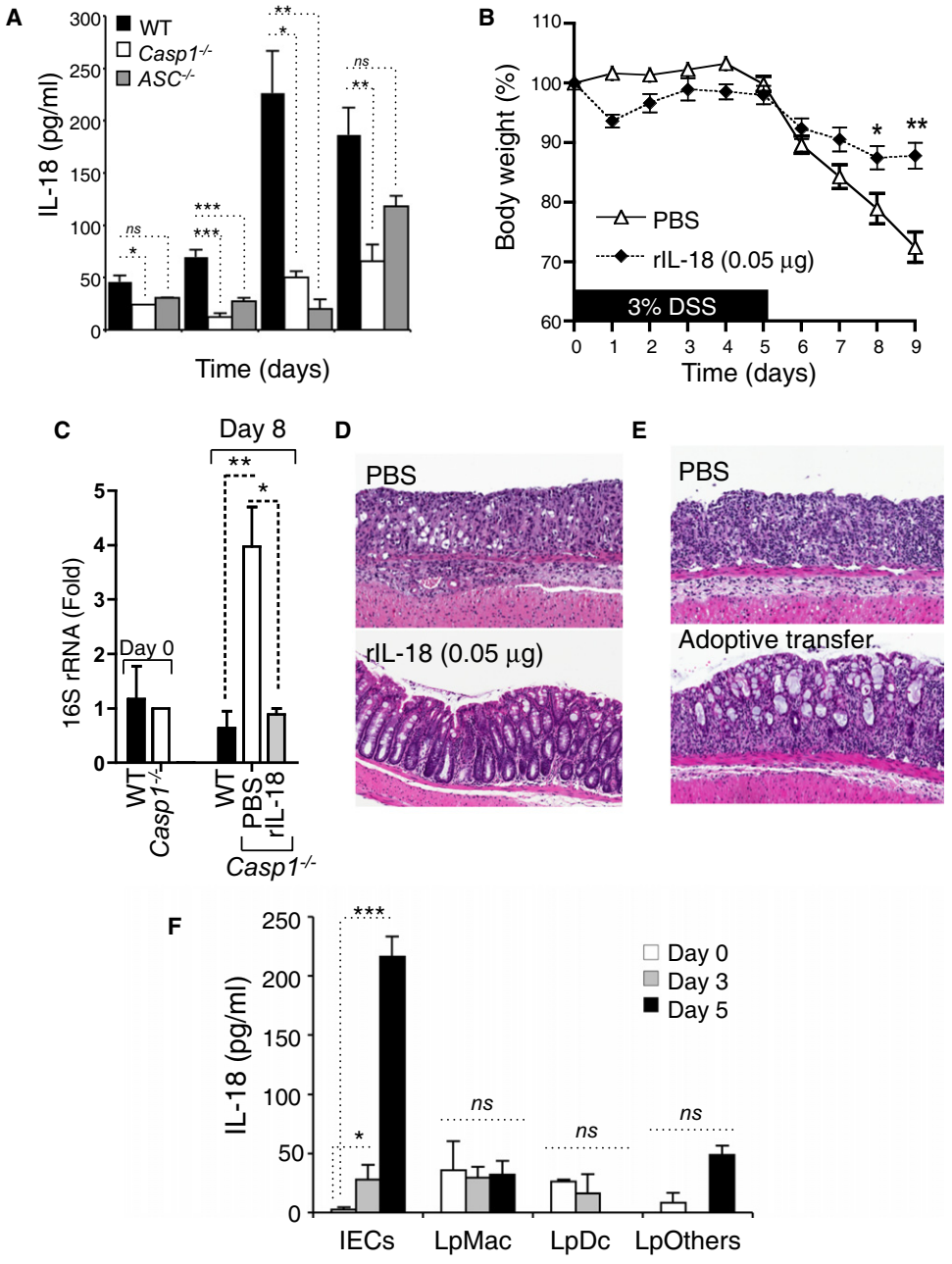

Figure 4. Exogenous IL-18 Administration Rescues *Casp1*$^{-/-}$ Mice from DSS-Induced Colitis

(A) IL-18 production in the serum of mice was determined by ELISA. Data represent the mean ± SEM. Student's t test was used for statistical analysis. *$p < 0.05$, **$p < 0.01$, ***$p < 0.001$; *ns*, nonsignificant.

(B) *Casp1*$^{-/-}$ mice were injected on days 0, 1, and 2 with either PBS or 0.05 μg recombinant IL-18 (rIL-18) and given 3% DSS as in Figure 1A. Body weight loss of mice treated with DSS and weighed daily is shown. Data represent the mean ± SEM (n = 4). Student's t test was used for statistical analysis; *$p < 0.05$, **$p < 0.01$.

(C) Quantitative real-time PCR of 16S rRNA in the colon. Data represent the means ± SEM. Student's t test was performed for statistical analysis. *$p < 0.05$, **$p < 0.01$.

(D) Hematoxylin and eosin (H&E) staining of colon sections derived from *Casp1*$^{-/-}$ mice treated with PBS or rIL-18 on day 9 post-DSS; (magnification 100×).

(E) Hematoxylin and eosin (H&E) staining of colon sections derived from *Casp1*$^{-/-}$ mice receiving PBS or adoptively transferred myeloid cells on day 9 after DSS; (magnification 100×).

(F) Quantification of ex vivo production of IL-18 by purified IECs and sorted lamina propria cells from untreated and DSS-treated colons. Data represent the mean ± SEM. Student's t test was used for statistical analysis. *$p < 0.05$, ***$p < 0.001$; *ns*, nonsignificant. IEC, intestinal epithelial cells; Lp, Lamina propria; Mac; macrophages; Dc, dendritic cells; and Others, all cells in Lp excluding macrophages and DCs that were purified by positive selection (see Experimental Procedures).

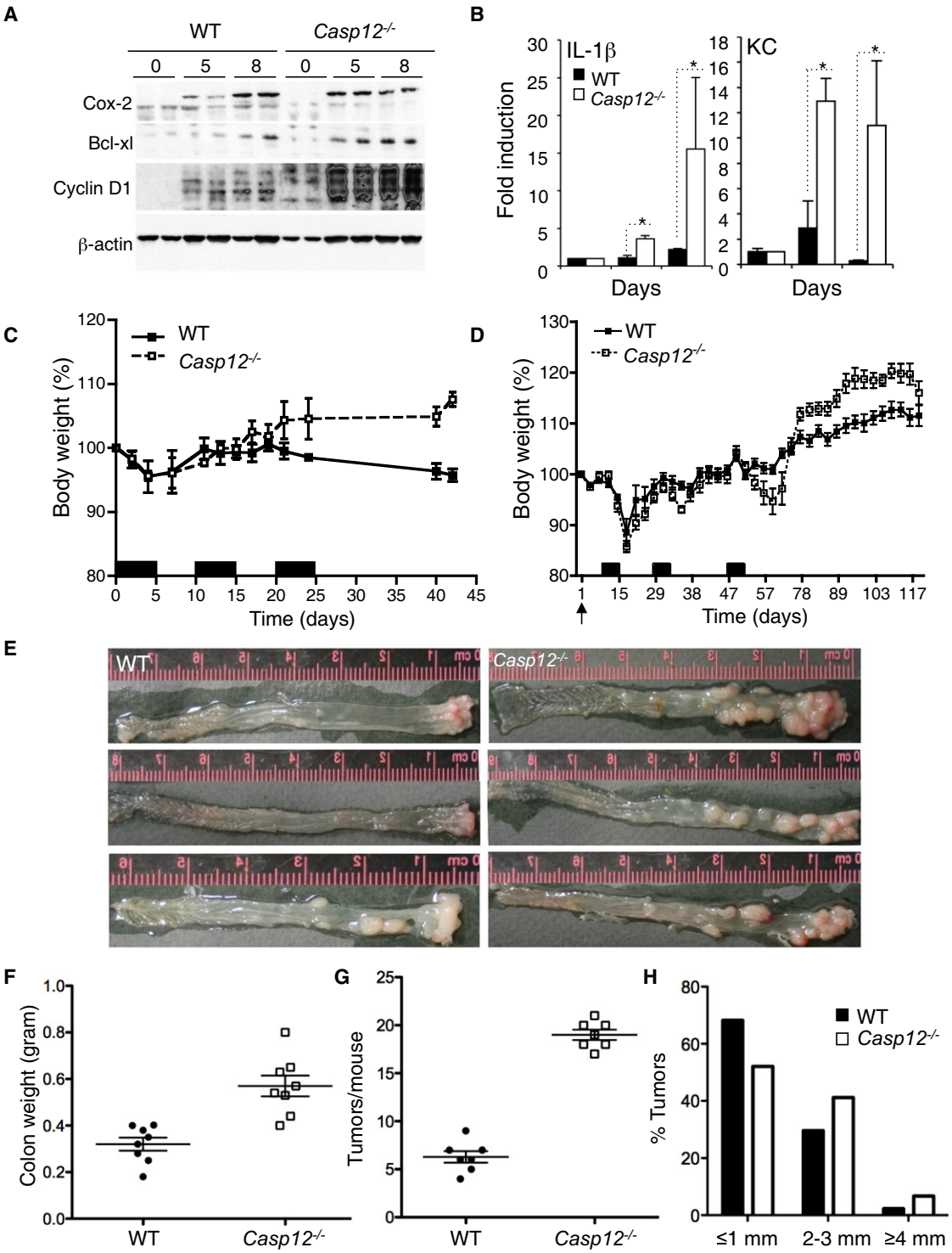

Figure 5. Enhanced Tumorigenesis in *Casp12*$^{-/-}$ Mice

(A) Immunoblot analysis of COX-2, Bcl-xl, cyclin D1, and IκBα in extracts of colon tissues derived from *Casp12*$^{-/-}$ mice as compared to WT mice on days 5 and day 8. β-actin was used to control for equal loading.

(B) RNA from the colons of WT and *Casp12*$^{-/-}$ mice was isolated at the same time points as in (A) and analyzed for KC and IL-1β expression by quantitative real-time PCR. Data represent means ± SEM of fold induction over untreated levels for each genotype (n = 3 per group). Student's t test was used for statistical analysis. *$p < 0.05$.

(C) Body weight curves of WT and *Casp12*$^{-/-}$ mice in a chronic model of DSS-induced colitis. Two percent DSS was given in the drinking water for three cycles of 5 days (black boxes) separated by 5 days of regular water. Mice were sacrificed on day 45.

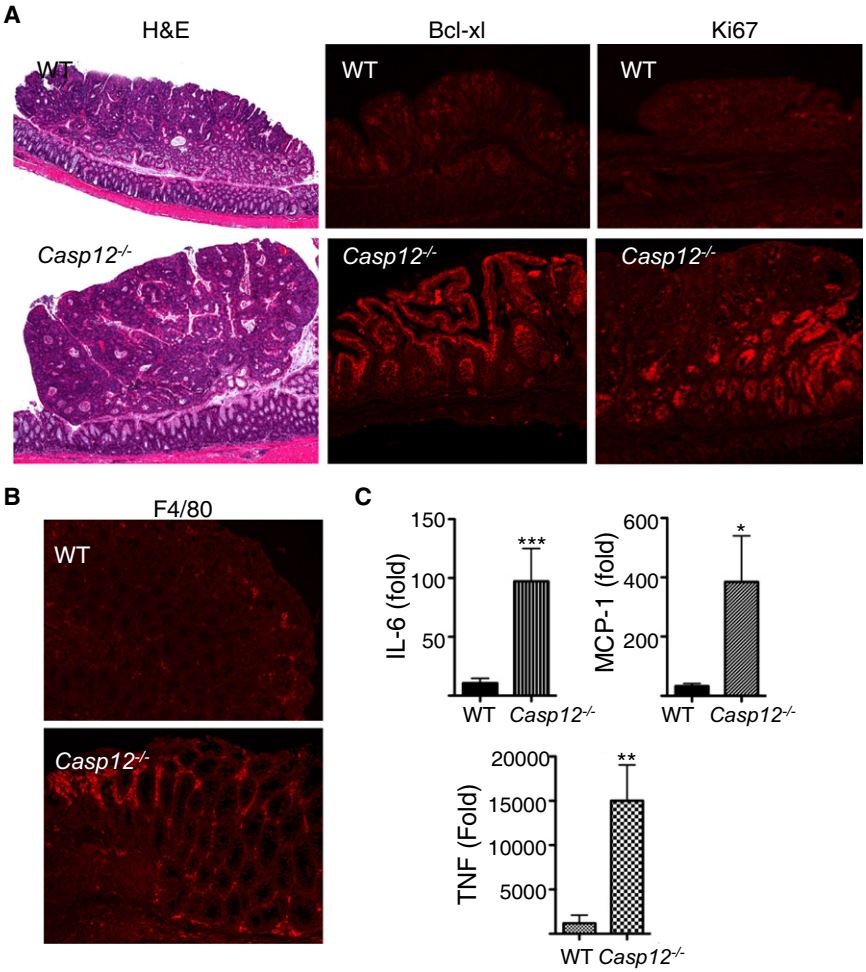

Figure 6. Caspase-12 Deficiency Increases Cell Survival and Proliferation

(A) H&E and immunofluorescence staining of the antiapoptotic protein Bcl-xl and proliferation marker Ki67 from colon tissue sections containing adenomas from WT and *Casp12*$^{-/-}$ mice.

(B) Immunofluorescence staining of macrophage infiltration with F4/80 antibodies.

(C) RNA was extracted from tumors derived from WT or *Casp12*$^{-/-}$ mice subjected to AOM+DSS after the third cycle of DSS. The expression of IL-6, MCP-1 and TNFα was examined by quantitative real-time PCR. Data represent means ± SEM of fold induction over untreated levels for each genotype (n = 7 per group). Student's t test was used for statistical analysis. *p < 0.05, **p < 0.01, ***p < 0.001.

Enhanced Expression of Tumor-Promoting Genes in *Casp12*$^{-/-}$ Mice

The colon histology of the AOM+DSS-treated mice was examined so that the effects of caspase-12 deficiency on intestinal homeostasis could be determined. Different types of adenocarcinomas had developed in WT and *Casp12*$^{-/-}$ mice including broad-based and pedunculated tumors (Figure 6A). However, the increased number and size of tumors in *Casp12*$^{-/-}$ mice compared to those in WT mice suggested that caspase-12 deficiency impacted on cell death, cell proliferation, or both. Because of the increased expression of Bcl-xl in the colon of *Casp12*$^{-/-}$ mice in response to DSS-induced colitis (Figure 5A), we investigated its expression pattern by immunohistochemistry in the AOM+DSS-induced tumors. Colon sections from *Casp12*$^{-/-}$ mice had a marked increase in Bcl-xl staining in intestinal epithelial cells, compared to colon sections derived from WT mice (Figure 6A). This result indicated that the enhanced tumorigenesis in *Casp12*$^{-/-}$ mice might be mediated by enhanced survival of intestinal epithelial cells partially through overexpression of the antiapoptotic gene *Bcl-xl*. In addition to its effects on cell survival, caspase-12-deficiency stimulated cell proliferation as revealed by increased Ki67 staining in tumors of *Casp12*$^{-/-}$ mice compared to WT tumors (Figure 6A). The enhanced proliferation and survival of the *Casp12*$^{-/-}$ intestinal epithelial cells is associated with increased inflammation in the colons of these mice compared to WT mice. Indeed, *Casp12*$^{-/-}$ colon tissue sections collected after the third cycle of DSS were studded with macrophages (F4/80^{+} cells) compared to sections from WT mice (Figure 6B) and had increased expression of the proinflammatory cytokines IL-6 and TNFα and the chemokine MCP-1 (Figure 6C). Altogether, these data suggested that *Casp12*$^{-/-}$ mice have an increased ability to recruit macrophages, which leads to increased production of inflammatory and tissue repair factors. Chronic activation of these pathways leads to enhanced cell proliferation, cell survival, and tumorigenesis. This result was corroborated by a genomic analysis of colitis-associated tumorigenesis in WT and caspase-12-deficient mice (Figure S4). A DNA microarray experiment with normal and tumor RNA from WT and

(D) Body weight curves of WT and *Casp12*$^{-/-}$ mice in an AOM+DSS model of colitis-associated CRC. After a single injection of azoxymethane ([AOM] 12.5 mg/kg) on day 0 (black arrow), 2% DSS was given in the drinking water for 3 cycles of 5 days (black boxes) separated by 2 weeks of regular water. Mice were sacrificed on day 123.

(E) Macroscopic view of the AOM+DSS-derived tumors in WT and *Casp12*$^{-/-}$ mice. Representative results from three independent animals are shown.

(F) Colons of WT and *Casp12*$^{-/-}$ mice were dissected, washed with PBS for removal of fecal content, cut longitudinally, and weighed.

(G) Tumor incidence induced by AOM+DSS in WT and *Casp12*$^{-/-}$ mice. Statistical analysis was performed with the Student's t test. ***p < 0.001. This experiment was repeated twice with similar results. In each experiment, a group of seven to ten mice was used per genotype.

(H) Size distribution of colonic tumors of WT and *Casp12*$^{-/-}$ mice. More than 50% of the tumors of *Casp12*$^{-/-}$ mice were larger than 1 mm in diameter as compared to 30% of the WT mice tumors.

Casp12$^{-/-}$ mice provided an overview of the variation in gene expression across these samples and showed a significant enrichment of genes mainly related to inflammation and immunity in the *Casp12*$^{-/-}$ mice tumors (Figures S4A and S4B). These included *Il1b*, *Il11*, *ccl7* (chemokine [C-C motif] ligand 7). and *tnfaip2* (TNFα-induced protein 2) (Figure S4C). Furthermore, the tumor gene set of *Casp12*$^{-/-}$ mice included genes involved in proliferation, angiogenesis, and metastasis, such as the transcription factor *ELK3*, which is regulated by the Ras/MAPK signaling pathway, *Icam1* (Intercellular adhesion molecule 1), *CD44* metastasis suppressor, and *col4a1* [collagen a_1(IV)] cell-matrix interaction molecule. Interestingly, relative gene expression of *Blm* (Bloom Syndrome gene), which is a major risk factor for colon cancer, was higher in *Casp12*$^{-/-}$ tumors compared to all other groups (Figure S4C). The microarray results provided an interesting gene signature associated with colitis-promoted CRC and corroborated the findings that *Casp12*$^{-/-}$ mice exhibited an increased inflammatory response after injury, a prerequisite to compensatory proliferation and cell survival, and such a response eventually leads to enhanced intestinal tumorigenesis.

DISCUSSION

A normal inflammatory reaction is self limiting because of various negative regulatory mechanisms induced to end the response (Coussens and Werb, 2002). These include anti-inflammatory cytokines and negative regulators of innate immunity and cytokine receptor pathways. When these molecular "brakes" are compromised, chronic inflammation ensues. The essential role of TLRs and NF-κB signaling in promoting tumorigenesis was highlighted by studies assessing onset of spontaneous CRC as well as colitis-associated CRC in targeted-gene deletion mouse models. These studies showed that deletion of MyD88 (Rakoff-Nahoum and Medzhitov, 2007) or IKKβ (Clevers, 2004) markedly reduced the incidence of tumor formation. In contrast, deletion of negative regulators of inflammation such as that of the *S*uppressors *O*f *C*ytokine *S*ignaling, SOCS1 (Hanada et al., 2006) or SOCS3 (Rigby et al., 2007), or of the dominant negative modulator of TLR-IL-1 receptor signaling SIGIRR (Xiao et al., 2007) resulted in higher tumor incidence. Here, we present results that show that deletion of caspase-12 resulted in higher tumor incidence. Our results indicate an essential contribution of the inflammasome-caspase-1-caspase-12 pathway in maintenance of intestinal homeostasis: a unique role for caspase-1 in tissue repair after injury and the control of the inflammatory response by caspase-12 contributes to immune tolerance in the gut.

Our results are in disagreement with a previous report showing resistance of caspase-1-deficient mice to acute and chronic colitis (Siegmund et al., 2001). This discrepancy may be attributable to differences in genetic background, gender of the animals used, and the microflora environment of the different animal facilities. The response of *Casp1*$^{-/-}$ mice to DSS in our experiments is highly similar to that of *Il18*$^{-/-}$, *Il18r1*$^{-/-}$. and *Myd88*$^{-/-}$ mice indicating one of two non-mutually exclusive possibilities: (1) that IL-18 is cytoprotective and that its signaling through MyD88 is critical to induce a tissue repair response after injury and (2) that TLRs and NLRs cooperate in inducing the signal to repair. Our results showing that exogenous administration of IL-18 rescued *Casp1*$^{-/-}$ mice from acute DSS injury are consistent with these two possibilities. The role of TLRs in tissue repair is linked to their ability to sense commensal bacteria in the colon. The cytosolic localization of NLRs renders them less accessible to commensal bacteria at the steady state. However, in response to a mechanical or chemical injury, invading commensals or bacterial products could reach the cytosol of both epithelial and myeloid cells. Furthermore, danger signals generated by tissue damage, such as excess ATP, are also known to stimulate NLRs and activate caspase-1.

Caspase-1 is activated within the inflammasome, and the best-characterized inflammasomes to date, namely NLRP1, NLRP3, IPAF, and NAIP5 inflammasomes, utilize the adaptor ASC to recruit and activate caspase-1 (Mariathasan and Monack, 2007). In addition to the role of ASC in the activation of the inflammasome, ASC has been reported to modulate NF-κB signaling in response to proinflammatory stimuli including TNFα and LPS (Stehlik et al., 2002). *Asc*$^{-/-}$ mice had a milder phenotype compared to *Casp1*$^{-/-}$ mice, which could be due to derepression of the NF-κB pathway.

Our results show that *Casp12*$^{-/-}$ mice were highly susceptible to sustained DSS treatment. This result is similar to what was observed in ATG16L1 null mice, in which the inflammasome was derepressed, as well as mice deficient in the dominant-negative modulator of TLR-IL-1 receptor signaling SIGIRR (Xiao et al., 2007), indicating that tight control of the caspase-1-IL-1R axis of inflammation is key to achieve immune tolerance in the gut and that deregulation of this pathway contributes to pathogenesis of inflammatory bowel diseases (IBDs).

Inflammatory bowel diseases, including ulcerative colitis and Crohn's disease, are associated with an elevated risk of CRC (Clevers, 2004), and here we showed that deregulation of the inflammatory caspase pathway underlies inflammation-associated tumorigenesis. C57Bl/6 mice are relatively resistant to tumorigenesis induced by the AOM+DSS regimen, developing five to six small adenomas at the most distal end of the colon. In sharp contrast, *Casp12*$^{-/-}$ mice had a drastic increase in tumor burden compared to caspase-12-proficient animals. Additionally, their tumors were larger and were distributed throughout the colon length. Using functional genomics, we established a molecular signature of inflammation-promoted CRC in the *Casp12*$^{-/-}$ mice, with evidence that genes involved in inflammation, immunity, and survival signaling are key to tumorigenesis.

In summary, we report a role of the inflammatory caspases in the regulation of tissue repair and immune tolerance to commensal microorganisms and provide a direct link between inflammatory caspase deregulation, colitis, and colitis-associated tumorigenesis. These results have important therapeutic implications for managing inflammatory bowel diseases and inflammation-associated colorectal cancer.

EXPERIMENTAL PROCEDURES

Animal Strains

Caspase-12 (*Casp12*$^{-/-}$)-, caspase-1 (*Casp1*$^{-/-}$)-, and ASC (*Asc*$^{-/-}$)-deficient mice on a C57Bl/6J background were bred and maintained at the McGill University Health Center. All animals used were 8–12 weeks old. All experiments were performed under guidelines of the animal ethics committee of McGill University (Canada).

Induction of Colitis

Experimental colitis was induced by adding DSS (55,000 kDa, MP Biomedical Cat# 160110) to the drinking water at a concentration of 3% (w/v). The animals were weighed daily and monitored for signs of distress as well as rectal bleeding. The scores for stool consistency were measured as in (Wirtz et al., 2007): (0) normal, (1) soft but formed, (2) very soft, (3) diarrhea, and (4) dysenteric diarrhea. Animals were treated either for 5 days and then allowed to recover by drinking water for additional 4 days or were treated continuously with DSS for 15 days. Blood was collected from mice with heart puncture. For the IL-18 rescue experiments, recombinant IL-18 (R&D, Cat#B002-5) was injected intraperitoneally at a concentration of 0.05 μg per mouse on days 0, 1, and 2 post-DSS. For the adoptive transfer experiments, spleenocytes extracted with Lympholyte-M (Cedarlane, Cat#CL5035) were depleted of T and B cells with anti-CD90.2 (Miltenyi biotech, Cat#130-049-101) and anti-CD19 (Miltenyi biotech, Cat#130-052-201), respectively, and injected intravenously at a concentration of 5–6 million cells/100 μl per mouse, on days 3, 4, and 5 post-DSS.

Isolation of Intestinal Epithelial Cells and Lamina Propria Cells

After dissection, colons were isolated and washed with cold RPMI (Wisent, Cat#350-000CL) supplemented with penicillin and streptomycin (Invitrogen, Cat#15140-122) and gentamycin (Invitrogen, Cat#15710-064). Colons were then cut into small pieces and incubated in RPMI containing antibiotics, 5 mM EDTA (Sigma, Cat#E5134), 3% FBS (Wisent, Cat#095-150), and 0.145 mg/ml DTT (Sigma, Cat#43817) for 30 min at 37°C with gentle shaking. For isolation of IECs, the supernatant was filtered in 100 μM strainers (Fisher, Cat#08-771-19) and centrifuged, and cells were resuspended in 30% (vol/vol) Percoll (Sigma, Cat#P4937). After centrifugation, the top layer was isolated, 100,000 cells were plated on collagen type I (VWR, Cat#CACB354236)-coated 96-well plates and cultured overnight. For the isolation of lamina propria cells, the remaining colon pieces were recovered and incubated in RPMI containing antibiotics, 0.1 mg/ml liberase TL (Roche, Cat#05401020001), and 0.05% DNase (Roche, Cat#10104159001) for 30 min at 37°C with gentle shaking. Supernatant was filtered with 70 μM strainers (Fisher, Cat#08-771-2). Dendritic cells and macrophages were then sorted with Pan DC (Miltenyi Biotec, Cat#130-092-465) and anti-CD11b (Miltenyi Biotec, Cat#130-049-601) microbeads, respectively. Cells were then cultured overnight in 96-well plates. The remainder of the lamina propria cells (consisting mostly of lymphocytes), labeled "others," were also cultured along with the IECs, macrophages, and DCs.

Induction of Tumorigenesis

Colitis-associated CRC was induced by injection of mice intraperitoneally, on day 0, with azoxymethane AOM (Sigma Cat#A2853) at a concentration of 12.5 mg/kg. On day 7, DSS was introduced in the drinking water at a concentration of 3% for 1 week, and 2 weeks of regular drinking water followed. The DSS treatment was repeated for two additional cycles but at a concentration of 2%. Mice were sacrificed on week 17; colons were removed from animals, flushed with cold PBS, and cut longitudinally. A picture of the colon was taken with a PowerShot G3 Digital Camera (Canon). The tumor size was measured with a caliper.

Quantitative Real-Time PCR

Two micrograms of total RNA was reverse transcribed with M-MLV reverse transcriptase (Invitrogen, Cat#28025-013) and random hexamers in a volume of 20 μl according to the manufacturer's protocol. The primers used for quantitative real-time PCR are listed in the Supplemental Information.

ELISA

Serum collected from mice and primary cell culture supernatants were examined for IL-18 and SAA concentrations with kits from R&D and Invitrogen, respectively.

Assessment of Intestinal Permeability

Intestinal macromolecular permeability was determined in mice by administering 400 μg fluorescein isothiocyanate (FITC)-dextran/g body weight as detailed in the Supplemental Information.

Histopathology and Immunohistochemistry

A histopathologist blindly assessed the level of colitis. The scoring system was as follows: (1) 1%–25%, (2) 26%–50%, (3) 51%–75%, and (4) 76%–100% based on the percentage of tissue affected by inflammation or crypt damage. Immunohistochemistry was performed on paraffin sections as detailed in the Supplemental Information.

Fluorescence In Situ Hybridization

Formalin-fixed paraffin-embedded sections were deparaffinized and rehydrated. Sections were incubated overnight at 37°C in the dark with Texas red-conjugated EUB338 general bacterial probe (5′-GCT GCC TCC CGT AGG AGT-3′) (Amann et al., 1990; Lupp et al., 2007) diluted to a final concentration of 2.5 ng/μL in hybridization solution (0.9 M NaCl, 0.1 M Tris [pH 7.2], 30% formamide, and 0.1% SDS). Sections were then washed once in the dark with hybridization solution for 15 min with gentle shaking. This step was repeated once with wash buffer (0.9 M NaCL, 0.1 M Tris [pH 7.2]), and sections were placed in dH_2O, mounted with ProLong Gold Antifade (Molecular Probes) that contains DAPI, and imaged as described above.

DNA Microarray

Total RNA was prepared from tissues and purified an RNeasy Mini kit (QIAGEN, Cat#74104) in accordance with the manufacturer's instructions. RNA quality was ensured with the Agilent Systems Bioanalyzer. Biotinylated RNA was prepared with an Illumina TotalPrep RNA amplification kit (Ambion, Cat#AMIL1791) and hybridized to Illumina Mouse Ref-8 Expression BeadChips. Mouse Ref-8 Expression BeadChip contains 24,000 well-annotated RefSeq transcripts. The McGill University and Génome Québec Innovation Centre performed RNA labeling, amplification, array hybridization, and scanning. Data obtained were analyzed with GeneSifter (Geospiza) and Cluster 3.0 (http://rana.lbl.gov).

Statistical Analysis

Data is represented as average ± standard error. Two-tailed Student's t test and ANOVA were used for evaluating statistical significance between groups. Kaplan-Meier was used for survival analyses.

ACCESSION NUMBERS

The microarray data are available in the Gene Expression Omnibus (GEO) database (http://www.ncbi.nlm.nih.gov/gds) under the accession number GSE20407.

SUPPLEMENTAL INFORMATION

Supplemental Information includes Supplemental Experimental Procedures, four figures, and one table and can be found with this article online at doi:10.1016/j.immuni.2010.02.012.

ACKNOWLEDGMENTS

This work was supported by grants from the Canadian Institute of Health Research to N.B., (MOP68984), to B.V., (MOP82801), and to M.S. and the Burroughs Wellcome Foundation to M.S. B.V. is the CHILD Foundation Research Scholar and a Canada Research Chair (Tier 2), and M.S. is a CIHR New Investigator. J.D.C. was supported by a Canadian Society for Immunology summer studentship and a McGill University Health Centre graduate studentship. We thank R. Flavell and V. Dixit for providing *Casp1*$^{-/-}$ and *Asc*$^{-/-}$ mice breeder pairs. We also thank P. D'Arcy and M.-L. Goulet for technical assistance and the McGill University and Génome Québec Innovation Centre for hybridization of the microarray.

Received: May 31, 2009
Revised: November 9, 2009
Accepted: December 31, 2009
Published online: March 11, 2010

REFERENCES

Amann, R.I., Krumholz, L., and Stahl, D.A. (1990). Fluorescent-oligonucleotide probing of whole cells for determinative, phylogenetic, and environmental studies in microbiology. J. Bacteriol. *172*, 762–770.

Balkwill, F., and Mantovani, A. (2001). Inflammation and cancer: Back to Virchow? Lancet *357*, 539–545.

Brown, S.L., Riehl, T.E., Walker, M.R., Geske, M.J., Doherty, J.M., Stenson, W.F., and Stappenbeck, T.S. (2007). Myd88-dependent positioning of Ptgs2-expressing stromal cells maintains colonic epithelial proliferation during injury. J. Clin. Invest. *117*, 258–269.

Clevers, H. (2004). At the crossroads of inflammation and cancer. Cell *118*, 671–674.

Coussens, L.M., and Werb, Z. (2002). Inflammation and cancer. Nature *420*, 860–867.

Hanada, T., Kobayashi, T., Chinen, T., Saeki, K., Takaki, H., Koga, K., Minoda, Y., Sanada, T., Yoshioka, T., Mimata, H., et al. (2006). IFNgamma-dependent, spontaneous development of colorectal carcinomas in SOCS1-deficient mice. J. Exp. Med. *203*, 1391–1397.

Kämpfer, H., Kalina, U., Mühl, H., Pfeilschifter, J., and Frank, S. (1999). Counterregulation of interleukin-18 mRNA and protein expression during cutaneous wound repair in mice. J. Invest. Dermatol. *113*, 369–374.

Kitajima, S., Takuma, S., and Morimoto, M. (1999). Changes in colonic mucosal permeability in mouse colitis induced with dextran sulfate sodium. Exp. Anim. *48*, 137–143.

LeBlanc, P.M., Yeretssian, G., Rutherford, N., Doiron, K., Nadiri, A., Zhu, L., Green, D.R., Gruenheid, S., and Saleh, M. (2008). Caspase-12 modulates NOD signaling and regulates antimicrobial peptide production and mucosal immunity. Cell Host Microbe *3*, 146–157.

Lupp, C., Robertson, M.L., Wickham, M.E., Sekirov, I., Champion, O.L., Gaynor, E.C., and Finlay, B.B. (2007). Host-mediated inflammation disrupts the intestinal microbiota and promotes the overgrowth of Enterobacteriaceae. Cell Host Microbe *2*, 204.

Mariathasan, S., and Monack, D.M. (2007). Inflammasome adaptors and sensors: Intracellular regulators of infection and inflammation. Nat. Rev. Immunol. *7*, 31–40.

Mariathasan, S., Newton, K., Monack, D.M., Vucic, D., French, D.M., Lee, W.P., Roose-Girma, M., Erickson, S., and Dixit, V.M. (2004). Differential activation of the inflammasome by caspase-1 adaptors ASC and Ipaf. Nature *430*, 213–218.

McIntire, C.R., Yeretssian, G., and Saleh, M. (2009). Inflammasomes in infection and inflammation. Apoptosis *14*, 522–535.

Nenci, A., Becker, C., Wullaert, A., Gareus, R., van Loo, G., Danese, S., Huth, M., Nikolaev, A., Neufert, C., Madison, B., et al. (2007). Epithelial NEMO links innate immunity to chronic intestinal inflammation. Nature *446*, 557–561.

Pegg, A.E. (1984). Methylation of the O6 position of guanine in DNA is the most likely initiating event in carcinogenesis by methylating agents. Cancer Invest. *2*, 223–231.

Pizarro, T.T., Michie, M.H., Bentz, M., Woraratanadharm, J., Smith, M.F., Jr., Foley, E., Moskaluk, C.A., Bickston, S.J., and Cominelli, F. (1999). IL-18, a novel immunoregulatory cytokine, is up-regulated in Crohn's disease: Expression and localization in intestinal mucosal cells. J. Immunol. *162*, 6829–6835.

Pull, S.L., Doherty, J.M., Mills, J.C., Gordon, J.I., and Stappenbeck, T.S. (2005). Activated macrophages are an adaptive element of the colonic epithelial progenitor niche necessary for regenerative responses to injury. Proc. Natl. Acad. Sci. USA *102*, 99–104.

Rakoff-Nahoum, S., and Medzhitov, R. (2007). Regulation of spontaneous intestinal tumorigenesis through the adaptor protein MyD88. Science *317*, 124–127.

Rakoff-Nahoum, S., Paglino, J., Eslami-Varzaneh, F., Edberg, S., and Medzhitov, R. (2004). Recognition of commensal microflora by toll-like receptors is required for intestinal homeostasis. Cell *118*, 229–241.

Reuter, B.K., and Pizarro, T.T. (2004). Commentary: The role of the IL-18 system and other members of the IL-1R/TLR superfamily in innate mucosal immunity and the pathogenesis of inflammatory bowel disease: Friend or foe? Eur. J. Immunol. *34*, 2347–2355.

Rigby, R.J., Simmons, J.G., Greenhalgh, C.J., Alexander, W.S., and Lund, P.K. (2007). Suppressor of cytokine signaling 3 (SOCS3) limits damage-induced crypt hyper-proliferation and inflammation-associated tumorigenesis in the colon. Oncogene *26*, 4833–4841.

Saitoh, T., Fujita, N., Jang, M.H., Uematsu, S., Yang, B.G., Satoh, T., Omori, H., Noda, T., Yamamoto, N., Komatsu, M., et al. (2008). Loss of the autophagy protein Atg16L1 enhances endotoxin-induced IL-1beta production. Nature *456*, 264–268.

Saleh, M., Vaillancourt, J.P., Graham, R.K., Huyck, M., Srinivasula, S.M., Alnemri, E.S., Steinberg, M.H., Nolan, V., Baldwin, C.T., Hotchkiss, R.S., et al. (2004). Differential modulation of endotoxin responsiveness by human caspase-12 polymorphisms. Nature *429*, 75–79.

Saleh, M., Mathison, J.C., Wolinski, M.K., Bensinger, S.J., Fitzgerald, P., Droin, N., Ulevitch, R.J., Green, D.R., and Nicholson, D.W. (2006). Enhanced bacterial clearance and sepsis resistance in caspase-12-deficient mice. Nature *440*, 1064–1068.

Siegmund, B., Lehr, H.A., Fantuzzi, G., and Dinarello, C.A. (2001). IL-1 beta-converting enzyme (caspase-1) in intestinal inflammation. Proc. Natl. Acad. Sci. USA *98*, 13249–13254.

Sivakumar, P.V., Westrich, G.M., Kanaly, S., Garka, K., Born, T.L., Derry, J.M., and Viney, J.L. (2002). Interleukin 18 is a primary mediator of the inflammation associated with dextran sulphate sodium induced colitis: Blocking interleukin 18 attenuates intestinal damage. Gut *50*, 812–820.

Stehlik, C., Fiorentino, L., Dorfleutner, A., Bruey, J.M., Ariza, E.M., Sagara, J., and Reed, J.C. (2002). The PAAD/PYRIN-family protein ASC is a dual regulator of a conserved step in nuclear factor kappaB activation pathways. J. Exp. Med. *196*, 1605–1615.

Takagi, H., Kanai, T., Okazawa, A., Kishi, Y., Sato, T., Takaishi, H., Inoue, N., Ogata, H., Iwao, Y., Hoshino, K., et al. (2003). Contrasting action of IL-12 and IL-18 in the development of dextran sodium sulphate colitis in mice. Scand. J. Gastroenterol. *38*, 837–844.

Villani, A.C., Lemire, M., Fortin, G., Louis, E., Silverberg, M.S., Collette, C., Baba, N., Libioulle, C., Belaiche, J., Bitton, A., et al. (2009). Common variants in the NLRP3 region contribute to Crohn's disease susceptibility. Nat. Genet. *41*, 71–76.

Watanabe, T., Asano, N., Murray, P.J., Ozato, K., Tailor, P., Fuss, I.J., Kitani, A., and Strober, W. (2008). Muramyl dipeptide activation of nucleotide-binding oligomerization domain 2 protects mice from experimental colitis. J. Clin. Invest. *118*, 545–559.

Wirtz, S., Neufert, C., Weigmann, B., and Neurath, M.F. (2007). Chemically induced mouse models of intestinal inflammation. Nat. Protoc. *2*, 541–546.

Xiao, H., Gulen, M.F., Qin, J., Yao, J., Bulek, K., Kish, D., Altuntas, C.Z., Wald, D., Ma, C., Zhou, H., et al. (2007). The Toll-interleukin-1 receptor member SIGIRR regulates colonic epithelial homeostasis, inflammation, and tumorigenesis. Immunity *26*, 461–475.

Yeretssian, G., Labbé, K., and Saleh, M. (2008). Molecular regulation of inflammation and cell death. Cytokine *43*, 380–390.